Computers & Fluids 73 (2013) 104–114

Contents lists available at SciVerse ScienceDirect

Computers & Fluids

journal homepage: www.elsevier.com/locate/compfluid

Reynolds-Averaged Navier–Stokes simulation of the heave performance of a two-body floating-point absorber wave energy system

Yi-Hsiang Yu, Ye Li *

National Wind Technology Center, National Renewable Energy Laboratory (NREL), Golden, CO 80401, USA

ARTICLE INFO

Article history:
Received 7 September 2011
Received in revised form 5 August 2012
Accepted 9 October 2012
Available online 17 October 2012

Keywords:
Wave energy conversion
Heave
Computational Fluid Dynamics
Reynolds-averaged Navier–Stokes equations
Point absorber
Power take-off

ABSTRACT

This paper presents a recent numerical study conducted by researchers at the National Renewable Energy Laboratory on a point absorber wave energy conversion (WEC) system using a Reynolds-averaged Navier–Stokes (RANS)-based Computational Fluid Dynamics (CFD) method. The device we studied was a two-body floating-point absorber (FPA) that operates predominantly in heave and generates energy from the relative motion between the two bodies. We performed a series of numerical simulation to analyze the hydrodynamic response and the power absorption performance of the system in regular waves. Overall, it was successful to use the RANS method to model the complex hydrodynamics interaction of the FPA system. We demonstrated the significance of the nonlinear effects, including viscous damping and wave overtopping. The study showed that the nonlinear effects could significantly decrease the power output and the motion of the FPA system, particularly in larger waves.

1. Introduction

The possibility of harnessing energy from ocean wave resources has gained interest in recent years, and reviews on wave energy conversion (WEC) can be found in Refs. [1–3]. To convert wave energy into useful power, a wide variety of WEC designs have been proposed, including oscillating water columns, bottom-hinged pitching devices, floating pitching devices, overtopping devices, and point absorbers. The history and the status of the technology development of WEC systems were comprehensively reviewed in Refs. [4,5]. The point absorber is regarded as one of the simplest WEC devices, and the energy capturing of the device is designed to be at its maximum when the system is close to resonance. A two-body floating-point absorber (FPA) system is the focus of this paper, which converts wave energy into electrical power based on the relative motion between the two bodies.

The possibility of using wave energy resources for generating power gained momentum in the 1970s during the oil crisis, and many studies on wave energy conversion of point absorber systems have been conducted by researchers since then. Early studies were focused on understanding the hydrodynamics of point absorbers and the maximum power that could be captured by the system. In particular, Budal and Falnes [6], Evans [7], Mei [8] and Newman [9] all proposed the concept of capture (or absorption) width simultaneously, which provided the theoretical limitation of power that an axisymmetric body can extract from waves. Later, Budal and Falnes [10] also suggested another power absorption limit based on the submerged-body volume. Based on similar analytical approaches, Falnes [11] showed that a two-body FPA system, using heave mode to extract energy from waves, can absorb the same amount of wave energy as a single-body point absorber system. Comprehensive reviews of these applied mathematical works were presented in Refs. [12,13].

To model point absorbers with more complicated geometries in non-extreme wave conditions, frequency domain methods are commonly used, where the hydrodynamic loads can be calculated using a boundary element method that solves the radiation and diffraction problems. Then, the dynamic response of the system and its power extraction performance can be obtained by solving the equation of motion in frequency or in time domain. In particular, this approach has often been used in the study of optimal control and tuning strategies for point absorbers [14–16]. Recently, Babarit et al. [17] used this approach to perform a series of studies on the power generation performance of eight selected WEC systems at several deployment site locations.

However, the effects of the nonlinear interaction between waves and the FPA device, particularly viscous damping and wave overtopping, are important to the dynamic response and the power generation performance of the system. In the frequency domain and time domain approaches, the viscous drag is often included through the use of empirical solutions, which may leads to significant uncertainty in the numerical prediction. Babarit et al. [17] showed that, if the coefficient was varied by a factor of 4, the effect

* Corresponding author.
E-mail address: ye.li@nrel.gov (Y. Li).

0045-7930/$ - see front matter © 2012 Published by Elsevier Ltd.
http://dx.doi.org/10.1016/j.compfluid.2012.10.007

on the power performance could be up to 30%. Therefore, to predict the power performance more accurately, a comprehensive study of a FPA device that considers nonlinear interactions by using Computational Fluid Dynamics (CFD) methods is needed. CFD methods have been widely used to model the complex nonlinear hydrodynamic wave and floating body interaction problems, including the analyses of several types of WEC systems [18–21]. For example, Agamloh et al. [18] modeled the dynamic response of the power extraction performance of a single-body heaving buoy, and the study was expanded to two buoys to investigate the effect of array system. Westphalen et al. [20] presented a series of studies on a floating pitching device and a platform that contained an array of power generation buoys by using different types of CFD codes, including a smoothed particle hydrodynamics method, a Cartesian cut cell-based artificial compressibility method, and two pressure-based Navier–Stokes codes.

For a two-body FPA system, the hydrodynamics is more complex. The problems involve the interaction between waves and the FPA system, including the floating part, the submerged part, the relative motion between the two and the effect of the power take-off (PTO) mechanism. We recently used a RANS-based CFD method to analyze a two-body FPA system. The FPA geometry used was inspired by Ocean Power Technologies' PowerBuoy (Fig. 1). Some preliminary results of the power extraction performance with a selected PTO damping were presented in Ref. [22].

To conduct a more systematic investigation of the FPA, researchers from the National Renewable Energy Laboratory (NREL) performed a series of numerical analyses using the RANS method and summarize the result in this paper. Specifically, this study aimed to investigate the nonlinear effect of the interaction between waves and the FPA system on the power generation performance. We describe the computational methodology and then present a series of studies on the hydrodynamic response of the two-body FPA system and its power absorption ability in regular waves with operational wave heights. The paper also includes grid-sensitivity analyses and validation studies, where the RANS simulation results were compared with the experimental data obtained from wave tank tests.

2. Modeling

2.1. RANS method

The unsteady incompressible flow field was described by the continuity equation and the Navier–Stokes equations,

$$\begin{aligned} &\nabla \cdot \mathbf{U} = 0, \\ &\rho(\mathbf{U}_t + \mathbf{U} \cdot \nabla \mathbf{U}) = -\nabla p + \mathbf{F}_b + \nabla \cdot \mathbf{T}, \end{aligned} \tag{1}$$

where ρ was the water density, $\mathbf{U}$ was the flow velocity vector, and $\mathbf{U}_t$ was its time derivative, $\mathbf{F}_b$ was the body force vector (e.g., gravity), and $\mathbf{T}$ was the stress tensor.

An unsteady RANS-based CFD model (STAR-CCM+[1]) was used, where the governing equations were discretized over a computational mesh using a finite volume method. A k–ω SST turbulence model was applied with a two-layer all y+ wall treatment model, and a second order implicit scheme was utilized for time marching. The transient SIMPLE algorithm was applied to linearize the equations and to achieve pressure–velocity coupling. A volume of fluid method (VOF) was applied to capture the free surface, and a mesh-morphing model was adopted to move and adjust the grids around FPA due to its dynamic motion. An arbitrary Lagrangian–Eulerian method was implemented to handle the cell movement and its deformation. The resulting system of algebraic equations was then solved using an algebraic multi-grid method. Note that the equation of motion calculation was coupled with the flow field simulation through iterations. The equation of motion was solved within the SIMPLE algorithm, where the dynamic response of the floating body was calculated by integrating (over time) the acceleration obtained from the equation of motion solution using an implicit algorithm. The body was then moved to a new position and the mesh was updated. The convergence of the coupling between the RANS simulation and the dynamics of the body was reached at each time step.

2.2. Response calculation

The dynamic motion of a floating-body was described by the equation of motions,

$$\begin{aligned} &m\mathbf{a} = \mathbf{F}, \\ &\mathbf{I}_g\mathbf{a}_\Omega + \boldsymbol{\Omega} \times \mathbf{I}_g\boldsymbol{\Omega} = \mathbf{M}, \end{aligned} \tag{2}$$

where m was the mass of the body, $\mathbf{a}$ was the acceleration vector for the translation, $\boldsymbol{\Omega}$ and $\mathbf{a}_\Omega$ were the angular velocity and acceleration vectors, $\mathbf{I}_g$ was the moment of inertia tensor at the center of gravity, $\mathbf{F}$ and $\mathbf{M}$ were the total force and moment vector acting on the body.

The two-body FPA system included two parts, a float and a reaction section, which were connected through a linear mass–spring–damper system to represent the PTO mechanism. Because the effect of mooring system on the power extraction performance can be negligible [23], it was not considered in the study. As the selected FPA system predominantly operates in heave, the FPA system is limited to single degree-of-freedom (heave) motion. Eq. (2) was then reduced to a one degree-of-freedom equation for each body. As a result, the equation of motion in heave for the float and the reaction section became

$$\begin{aligned} &\text{Float} : m_F\mathbf{a}_F = (F_z)_F + F_{\text{PTO}}, \\ &\text{Reaction section} : m_R\mathbf{a}_R = (F_z)_R - F_{\text{PTO}}, \end{aligned} \tag{3}$$

where F_{PTO} was the PTO force, and F_z was the force component in heave. Subscripts 'F' and 'R' indicated the float and the reaction section, respectively. F_{PTO} was represented by a spring-damper force, which was

$$F_{\text{PTO}} = -C_{\text{PTO}}(u_F - u_R) - K_{\text{PTO}}(z_F - z_R) \tag{4}$$

where K_{PTO} was the spring stiffness, C_{PTO} was the power absorption (damping) coefficient, u_F and u_R are the heaving velocity of the float and the reaction section and z_F and z_R were the heaving displacement of the float and the reaction section.

Fig. 1. A prototype of OPT's PowerBuoy wave energy generation system. NREL PIX # 17114.

[1] STAR-CCM+ is a commercial CFD package, developed by CD-adapco.

2.3. Domain and boundary conditions

Fig. 2 shows the computational domain and domain boundaries of the numerical wave tank used in the RANS simulations. The computational domain was 100 m wide ($0\,\text{m} \leqslant y \leqslant 100\,\text{m}$), 170 m high ($-70\,\text{m} \leqslant z \leqslant 100\,\text{m}$), and 7 wavelengths long ($-2\lambda \leqslant x \leqslant 5\lambda$). The seabed was given at 70 m below the mean water surface, and a 5th-order Stokes wave velocity profile was specified at the inflow and top boundaries. The pressure outlet was implemented at the down wave boundary, and a symmetry boundary was placed along the x–z plane to reduce the size of the problem (note that the effect of the domain width was also studied and will be discussed in a later section). To absorb the outgoing and reflecting waves without creating additional numerical disturbance, a sponge-layer method was applied, in which a damping zone (2λ in the wave propagation direction) was placed in front of the down wave boundary.

3. Locked FPA modeling

A series of studies was first performed by using a locked FPA model, where the float and reaction section moved in transient as a single body. Therefore, the equation of motion for the locked FPA model became:

$$m\mathbf{a}_z = F_z, \tag{5}$$

where $\mathbf{a}_z$ was the acceleration of the locked FPA device in heave. The work was conducted for grid-sensitivity analysis and investigating the hydrodynamic performance of the system without the consideration of power extraction.

3.1. FPA geometry and dimensions

Fig. 3 shows the geometry and the dimension of FPA model used in the wave tank test and the RANS simulations. In the RANS simulation, we only considered a basic structural design, where the FPA model geometry neglected the supporting jacket and the details of the reaction plate. The mass of the full-scale single body model used in the RANS simulations (unless mentioned otherwise) was about 249 metric tons with the center of gravity located 22.4 m below the mean free surface. Note that the device design included a set of ballast tanks in the reaction section to keep the center of gravity below the center of buoyancy to maintain stability.

3.2. Grid generation and resolution studies

The meshes were created using the STAR-CCM+ grid generation utility. Fig. 4 shows the grid resolution around the FPA model. The grid resolution was finer near the free surface and around the FPA to capture both the wave dynamics and the details of the flow around the FPA. In addition, prism-layer cells were placed along the FPA surface, and the height of the first layer was set so that the value of $y+ (30 \sim 100)$ satisfied the turbulence model requirement. Note that the grid sensitivity studies were performed to ensure the convergence of the RANS solutions was reached and grid resolution was sufficient for the following hydrodynamics analysis.

The grid size Δx (in the wave propagation direction) was determined by the incident wavelength, and the grid size Δz (in the vertical direction) near the free surface was adjusted according to the wave height H. A series of two-dimensional (2D) numerical wave tank tests was conducted, without the presence of the absorber, to determine the appropriate grid resolution needed to model the wave dynamics. A 5th-order Stokes wave with a height of 10 m and a period of 17.5 s was given, where the wave was in the range of intermediate water waves (depth to λ ratio ≈ 0.18). The peak-to-trough wave elevation (H_{pt}/H) was evaluated to investigate the effect of grid resolution on wave dynamics modeling, and the quantity is plotted against the grid size in Fig. 5. It appeared that a grid resolution of $\Delta x < \lambda/80$ and $\Delta z \approx H/20$, near the free surface, sufficient.

To study the appropriate grid resolution around the FPA model and domain width, five grids with different resolutions and sidewall distances were generated. An incident wave profile with a height of 2 m and a period of 10 s was given. The statistics for each grid are summarized in Table 1. The heave response was evaluated to quantitatively analyze the effects of grid resolution and the domain width on the hydrodynamics of the FPA model. The normalized heave response (Heave/H) is plotted verses grid resolution in Fig. 6. The domain width study indicated that the effect of the sidewall distance was not significant, particularly when it was greater than 9 R_{FPA} (less than 1%). Further, the local grid resolution around the FPA model had little effect (3%) on the prediction of the amplitude of the heave response, as shown in Fig. 6. However, using grid 1 would result in a phase shift on the prediction of the response, which would affect the accuracy in predicting the resonance frequency of the system. Therefore, it was considered to be too coarse to use.

In addition, the study showed that a grid with resolution and sidewall distance similar to grid 2 was sufficient for the following analysis, and the total number of cells for grid 2 was on the order of 1.6 million. Note that if the FPA model was allowed to move in

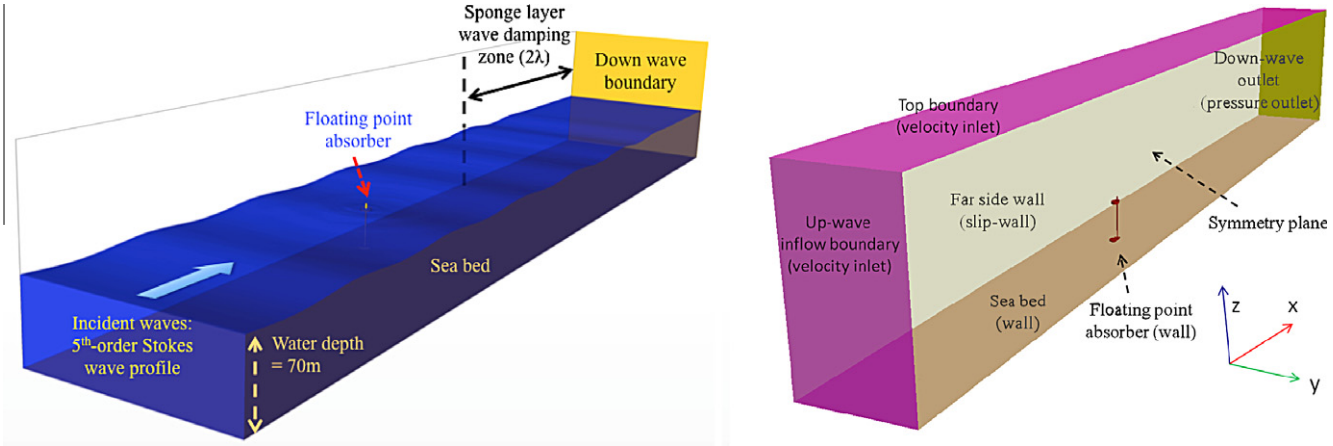

Fig. 2. Computational domain and domain boundaries.

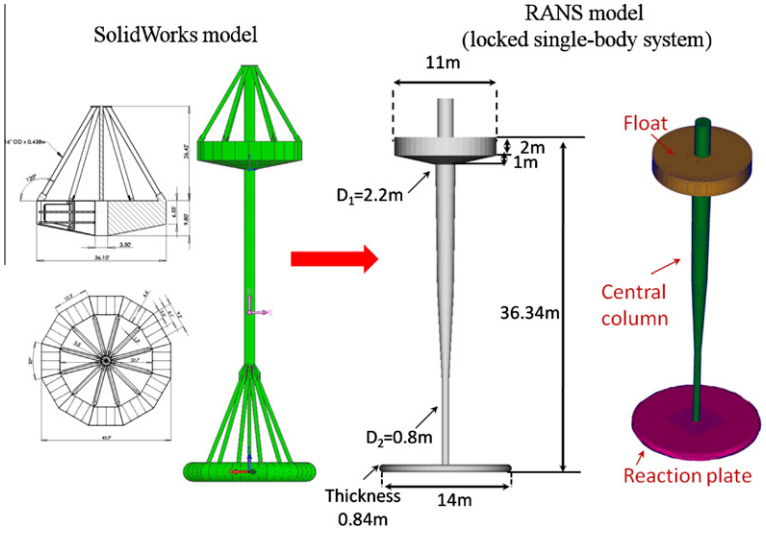

Fig. 3. FPA geometry and dimensions.

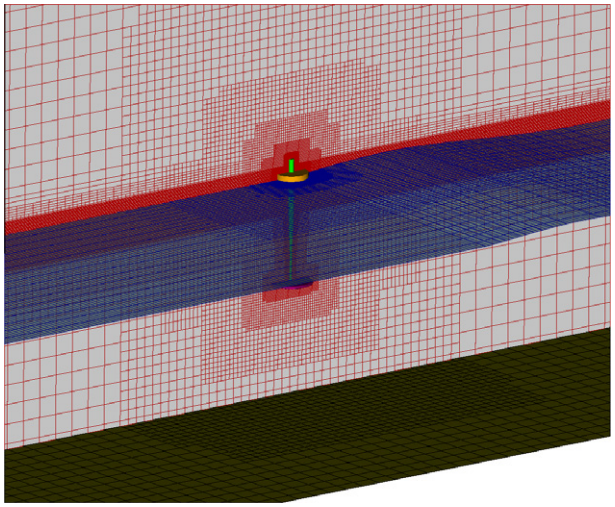

Fig. 4. Grid around the single-body point wave absorber model.

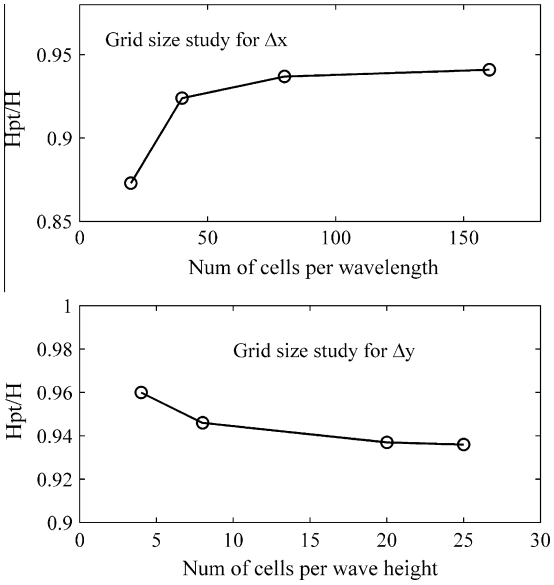

Fig. 5. Effect of grid resolution on wave dynamics modeling.

other degree-of-freedom, particularly in rotational motions, the viscous damping effect caused by those shed vortices around the FPA might have been more significant and retained the motions. In that case, the detail of the flow needs to be further resolved, and a higher resolution grid may be required.

To keep the Courant number small to preserve the numerical stability, a small time step of $T/400$ was utilized in the study, where T was the incident wave period. All the RANS simulations were carried out on NREL's high-performance computing (HPC) system.[2] For a mesh with 1.6 million elements, it took about 24 h on 48 cores to complete 8 wave periods of time (3200 time steps).

3.3. Heave decay test

In December 2010, an experimental test was performed at UC Berkeley's wave tank to validate the numerical prediction. Fig. 7 shows the 1/100-scale model used in the test and the dimensions of the tank, where the tank is 68 m long, 2.4 m wide and 1.5 m deep. The 1/100-scale model was built based on the SolidWorks design shown in Fig. 3. A 2D motion tracking system was utilized to capture the FPA motion, and the system used passive markers on the buoy to create targets for the motion tracking software. The motions were captured as a 2D projection, orthogonal to the direction of wave propagation in the tank.

Note that after including the weight of the load cell and the tracking target, the total mass of the 1/100-scale FPA model in the experimental test was 313 g. The mass of the FPA model in the RANS decay test was adjusted to match the experimental decay test. The computational domain was 1.7 m high ($-0.7\text{ m} \leqslant z \leqslant 1\text{ m}$), 8 m long ($-4\text{ m} \leqslant x \leqslant 4\text{ m}$), and 4 m wide ($0\text{ m} \leqslant y \leqslant 4\text{ m}$), where a symmetry boundary was placed along the x–z plane. Because the computational domain for the decay test was wider in the y-direction, the total number of elements used in the RANS simulation was around 2.3 million elements, with a resolution similar to grid 2. A sponge-layer damping zone was placed in front of all the far field boundaries to absorb the outgoing waves. To perform the decay test, the FPA was lifted with an initial displacement of $H_{in} = 0.02$ m (model scale). Fig. 8 shows the heave decay time history obtained from the RANS simulation and the

[2] Each compute node consisted of dual socket/quad-core 2.93 GHz Intel Nehalem processor, with 12 GB of memory shared by all eight cores.

Table 1
Computational grid statistics.

Grid No.	Number of cells	Approx. grid resolution on the body surface (cm)	Sidewall distance
1	0.5×10^6	100	18 R_{FPA}
2	1.6×10^6	50	18 R_{FPA}
3	2.8×10^6	25	18 R_{FPA}
4	0.8×10^6	50	9 R_{FPA}
5	5.0×10^6	50	36 R_{FPA}

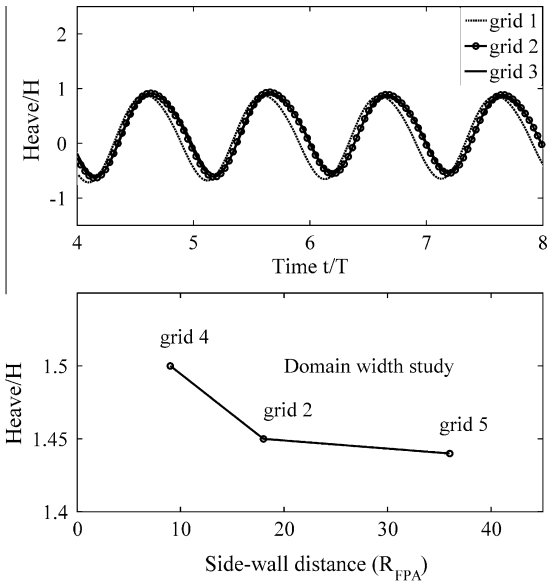

Fig. 6. Effects of the grid resolution and the domain width on the FPA heave response.

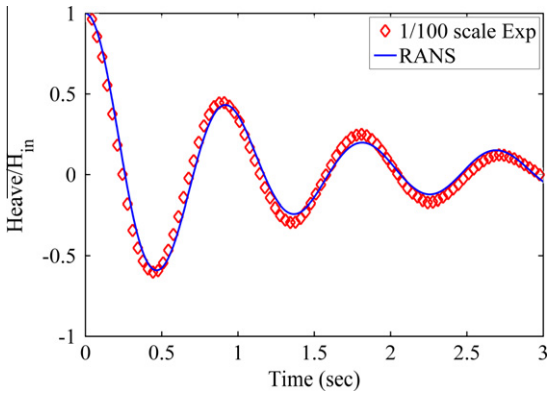

Fig. 8. Heave decay from RANS and from the experimental measurement.

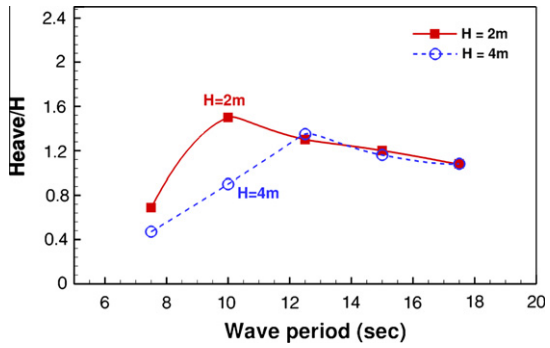

Fig. 9. Comparison of the FPA response in heave (scaled by H) in 2 m and in 4 m waves.

experimental measurement. The RANS result agreed with the experimental data, and the natural decay period was found to be around 0.9 s (9 s in full scale).

The grid-sensitivity analysis, which was presented in a previous section, and the validation decay test study, which was conducted by comparing the RANS solutions to the experimental results, indicated that the mesh and specified numerical settings and algorithms were sufficient and capable of being used to model the FPA system in following studies.

3.4. Regular waves analysis

A series of locked FPA RANS simulations was performed to investigate the nonlinear effects of the interaction between waves and the absorber under regular waves without the present of PTO mechanism. The response amplitude operators (RAOs) of two different incident wave heights, 2 m and 4 m, are plotted in Fig. 9. The results that the RAO under 2 m waves had a peak period close to the natural period obtained from the decay test. The amplitude was reduced and the peak period shifted to T = 12.5 s in 4 m wave scenarios. The shift indicated that the system was subject to a larger damping in larger waves. Fig. 10 plots an example of the water surface and the hydrodynamic pressure contour at a selected time instant. Note that wave overtopping barely occurred in the 2 m wave scenarios. However, it was often observed in the 4 m-wave.

As mentioned in Ref. [22], when the wave period is sufficiently longer than the resonant period, the heave response follows the motion of the water surface, and the heave response is almost equal to the incident wave height. When the wave period is shorter, a phase shift between the wave elevation and the floating-body

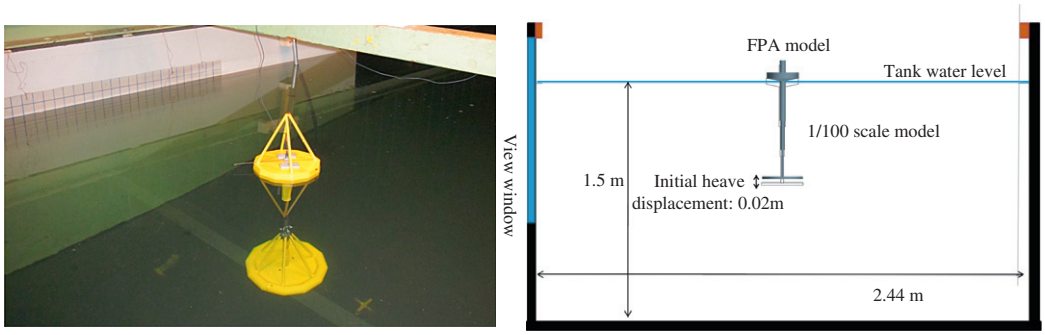

Fig. 7. The single body FPA model in the experimental wave tank and the tank dimensions.

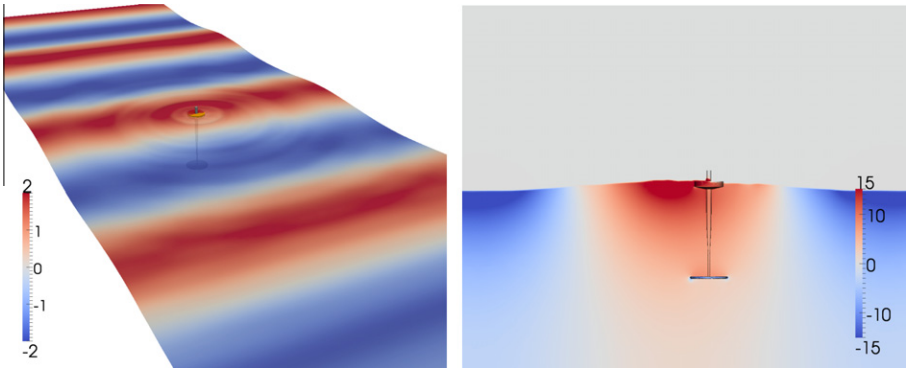

Fig. 10. Water surface and the hydrodynamic pressure contour at $t/T = 6.2$ ($H = 4$ m; $T = 10$ s).

heave motion occurs, and the phase shift increases with decreasing wave period. Therefore, the nonlinear effects can be more significant when the wave period is shorter, particularly in larger wave-height scenarios. It was anticipated that the nonlinear effects of wave and floating-body interaction introduced additional damping forces that reduced the response amplitude and shifted the peak period of the FPA system.

4. Two-body FPA in waves

The hydrodynamics of the two-body FPA system is more complex than a single-body point absorber system, where the power generation performance depends on the relative motion between the float and the reaction section. Therefore, a series of RANS simulations was performed to investigate the power extraction potential of the FPA system, and the results were compared with experimental measurement data for validation.

4.1. FPA model and numerical settings

The numerical settings and the mesh resolution used in the two-body FPA RANS simulation were similar to those used in the locked FPA simulations. Fig. 11 shows the model geometry and dimension of the two-body FPA system used in the RANS simulation. Given that the two-body FPA system generally converts energy from the relative heave motion between the two oscillating bodies, the FPA model used in the RANS simulations was further modified form the original one (Fig. 3). The FPA was separated into a float and a reaction section. The reaction section was fully submerged and nearly to neutrally buoyant. The central column diameter was modified to maintain an immersed volume and a center of buoyancy close to the original FPA model. The float and the reaction section weighed 84.5 metric tons and 165 metric tons. The two sections were connected through the use of a mass–spring–damper system, which was used to model the PTO mechanism. Note that the spring was mainly utilized to connect the two bodies, and a small value of 20 kN/m was specified to keep the reaction section in position. The power absorption coefficient was a specified constant in each numerical simulation. The instantaneous power was proportional to the square of the relative translational velocity of the two sections, which was defined as

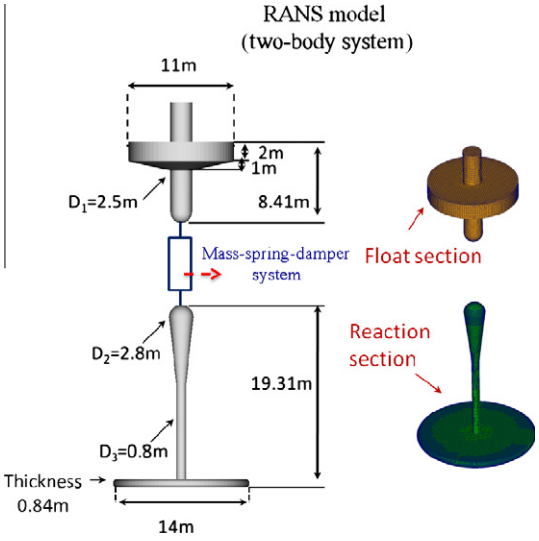

Fig. 11. Two-body FPA model in RANS.

$$P_{\mathrm{PTO}} = C_{\mathrm{PTO}}(u_F - u_R)^2. \tag{6}$$

The time-averaged power was calculated by integrating the instantaneous power over the time, and the value was averaged from the last five wave periods of time, where the response coincided with the stationary periodic solution.

4.2. Experimental wave tank test

In August 2011, an experimental test was performed at UC San Diego Scripps Institution of Oceanography's wave tank. Fig. 12 shows the wave tank dimension and the experimental settings. A 1/33-scale model was used in the test, where the float and the central column were connected with a miniature hydraulic cylinder in a closed circuit with a needle valve to provide damping to the relative motion to represent the PTO mechanism. The PTO force was obtained from a load cell measurement. In addition, a three-dimensional (3D) camera tracking system was used to verify the linear potentiometer measurement quality. More details of the experimental design and settings were described in Ref. [24].

4.3. Response in regular waves

Fig. 13 shows an example of the heave response of the float and reaction section with two different PTO damping coefficient values. Because the motion of fluid particles decreased rapidly with increasing depth below the free surface, the wave excitation force on the float was more significant than on the reaction plate. Therefore, the heave motion of the float was expected to be greater than that of the reaction section. The relative motion between the two bodies was reduced when wave energy was extracted by the PTO mechanism, and it decreased as the power absorption coefficient

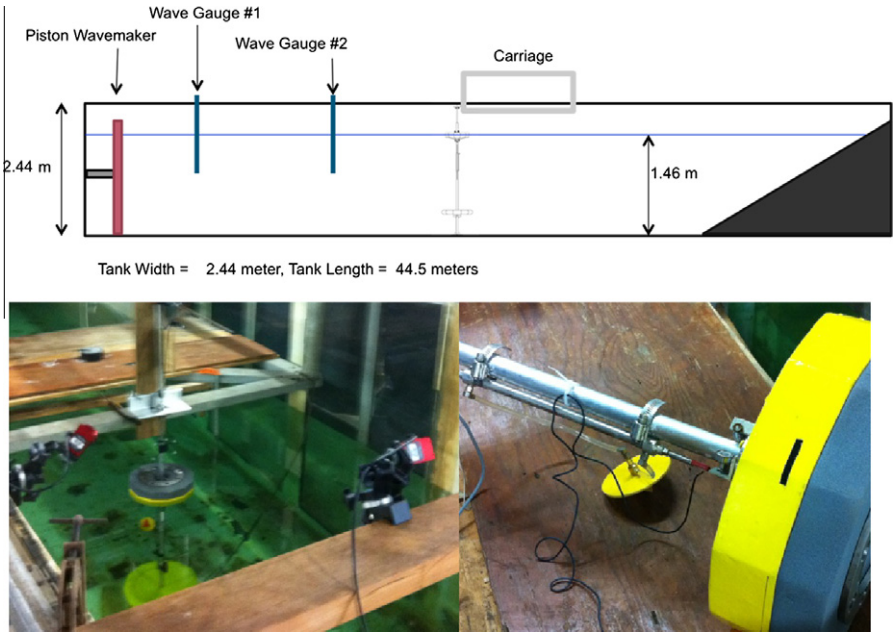

Fig. 12. Experimental wave tank test model dimension and settings.

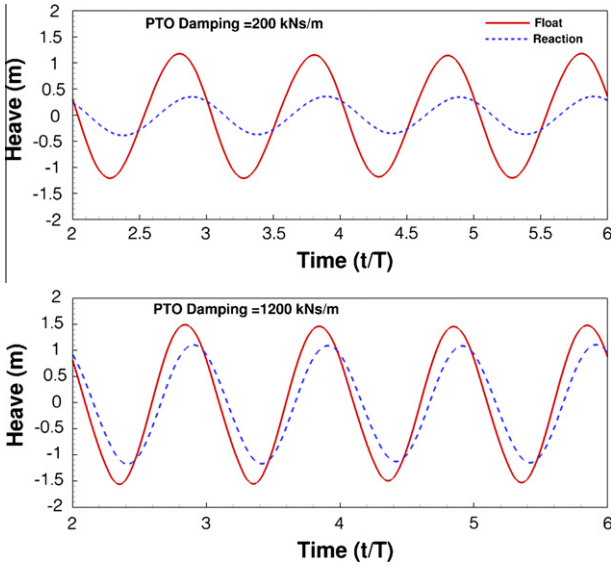

Fig. 13. Heave response of the float and the reaction sections ($H = 2.5$ m; $T = 10$ s).

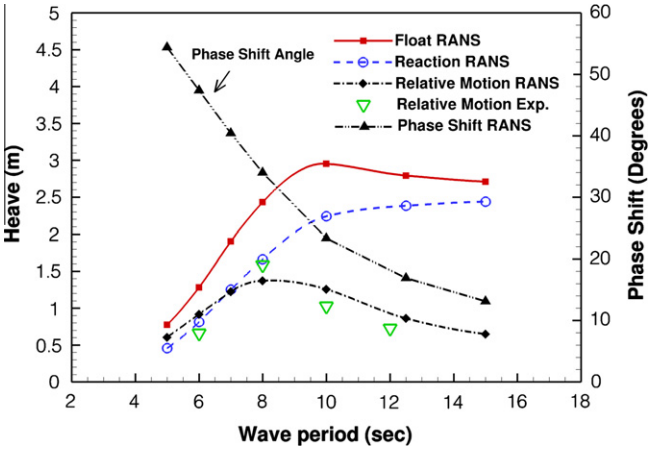

Fig. 14. Hydrodynamic response of the FPA system ($H = 2.5$ m).

increased. In addition, a phase shift between the history response of the float and the reaction section was observed. The result showed that the hydrodynamic responses of the float and the reaction section were affected when the PTO mass-spring-damper system was installed.

Fig. 14 shows an example of the heave response of the FPA system in 2.5 m waves with a PTO absorption coefficient of 1200 kNs/m. The figure shows the heave response of the float and the reaction section, the relative motion and the phase shift between the two bodies, where the values were plotted against the wave period. The float had a peak period around $T = 10$ s. The reaction section, on the other hand, gradually increased with the incident wave period, and there was no peak in the response of the reaction section, suggesting that the reaction section was over-damped. Note that the viscous drag, as a result of flow separation and vortex shedding, was the dominant damping source for the reaction section, as the radiation damping force on the reaction section was negligible. In addition, the phase shift between the float and the reaction-section varied with the incident wave period. The angle was decreased as the incident wave period increased. The phase shift between the float and the reaction section resulted in the relative motion having a peak period around $T = 8$ s, which was different from the peak period of the float.

The RANS simulations were also compared with the measurement data obtained from the experimental wave tank test, and the RANS results agreed fairly well with the experimental data. The slight difference could be attributed to the difference of the model geometry. In particular, the FPA model used in the experimental test had a larger float height as compared to the one used in the RANS simulation. As a result, in the experimental wave tank test, wave overtopping did not occur as often as we observed in the RANS simulations. It was anticipated that wave overtopping could result in an additional damping force that restrained the FPA motion.

Figs. 15 and 16 plot the free surface elevation contour and the hydrodynamic pressure distribution at selected times. The wave height was 4 meters and the wave period was 7 s, which was

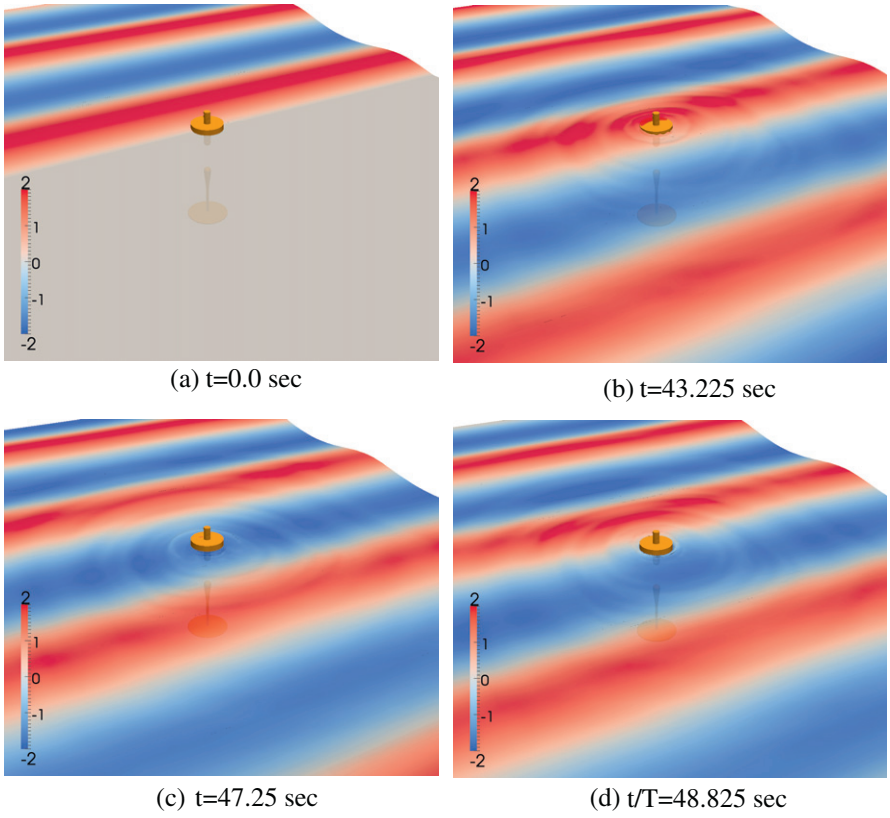

Fig. 15. Free surface elevation around the two-body FPA.

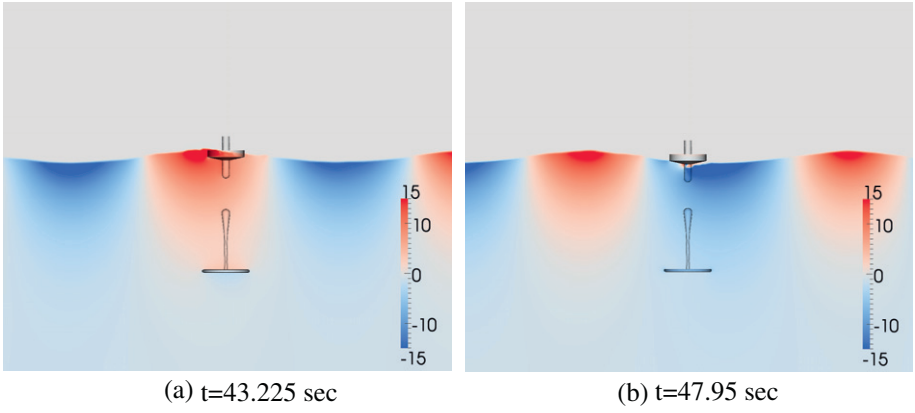

Fig. 16. Hydrodynamic pressure (kPa) contour (H = 4 m).

smaller than the peak period of the FPA system. Similar to the locked-body FPA scenarios, wave overtopping was observed, and the float could be completely out of water because of the small daft of the float and the phase shift between the float response and the wave elevation. In addition, the result showed a ring-shaped outgoing wave, which was mentioned in the study of Budal and Falnes [6].

4.4. Power generation

Generally, an FPA system has an optimal power absorption coefficient value for each wave conditions that provides the system the maximum power, where the optimal value varies for different wave periods and wave heights. Figs. 17 and 18 plot the power extraction performance of the FPA system in 2.5 m and 4 m waves

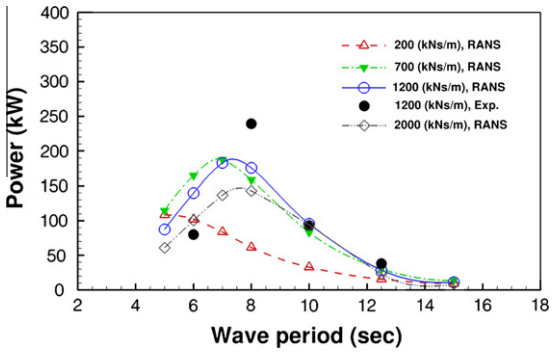

Fig. 17. Power absorption performance of the FPA system in 2.5 m waves.

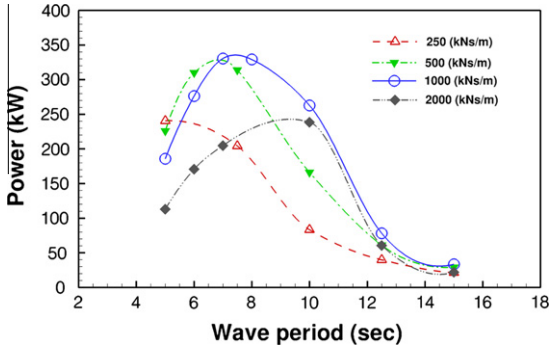

Fig. 18. Power absorption performance of the FPA system in 4 m waves.

against the incident wave period with a range of power absorption coefficients between 200 kNs/m and 2000 kNs/m. The RANS prediction was also compared to the experimental measurements in the 2.5 m wave scenario. The RANS results agreed with the experimental data, except at the resonance, where the peak response occurred and wave overtopping was essential. It was anticipated that the slight difference on the power extraction performance prediction might have been attributed to the difference in the model geometry, as discussed in the last section. For the cases we tested, the FPA system had an optimal power extraction performance when the power absorption coefficient was in the range between 700 kNs/m and 1200 kNs/m. For example, the FPA system was able to generate 325 kW of time-averaged power under 4 m waves when the power absorption coefficient was equal to 1000 kNs/m.

Fig. 19 plots the instantaneous power history of the FPA system with the power absorption coefficients of 200 kNs/m and 1200 kNs/m. The time history of the FPA system power generation shows that the system can contain high peaks and low peaks, depending on if the FPA system is moving upward or moving downward. The results suggest that the nonlinear interaction between waves and the floating device can influence the dynamic response of the system as well as the power performance even in small wave scenarios. The nonlinearity increases when a larger power absorption coefficient is selected.

5. Discussion

We here compared our RANS results to those obtained from analytical solutions and a potential flow numerical solution to quantify the power generation efficiency of the FPA system. Falnes

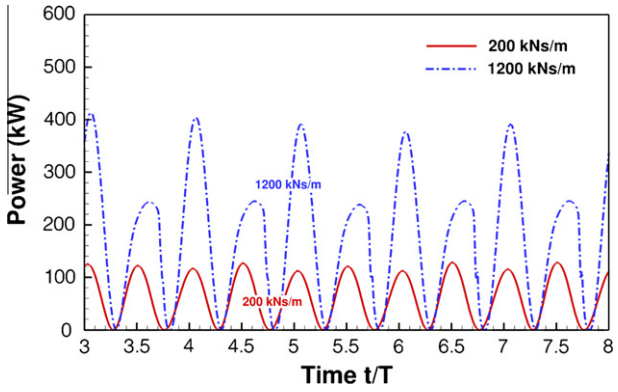

Fig. 19. An example of instantaneous power performance history.

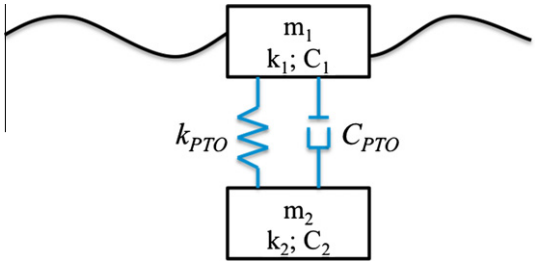

Fig. 20. A schematic representation of the two-body FPA WEC system (K_{PTO} = 0 kN/m).

[11] showed that, for a two-body axisymmetric system, it is also possible to extract the same amount of wave energy as a single-body system, which has a capture width of $\lambda/2\pi$ in ideal potential flow. Therefore, the maximum wave power P_{max} that a two-body system can absorb is

$$P_{max} = \frac{F_d^2}{8C} = JL_{max}, \tag{7}$$

where F_d is the excitation force, C is the radiation damping, J is the wave energy flux, and L_{max} is the absorption (capture) width. It was noted that the solution obtained from Eq. (7) assumed that the natural frequency of the point absorber was always tuned and matched the incident wave frequency perfectly.

For a given FPA geometry, it is clear that the FPA system will be less efficient when the system is not close to the resonant. Therefore, we modeled the two-body FPA system by solving the radiation and diffraction problems to obtain the potential flow power generation limit for the system. Fig. 20 shows the schematic representation the two-body FPA WEC system, where K_{PTO} was equal to zero in the study. The equation of motion for the two-body FPA system, Eq. (3), in heave can be re-written as

$$\begin{aligned}&\text{Float}: (m_F + A_F)\ddot{Z}_F + k_F Z_F + C_F \dot{Z}_F + C_{PTO}(\dot{Z}_F - \dot{Z}_R) = (F_d)_F,\\ &\text{Reaction section}: (m_R + A_R)\ddot{Z}_R + k_R Z_R + C_R \dot{Z}_R + C_{PTO}(\dot{Z}_R - \dot{Z}_F) = (F_d)_R,\end{aligned} \tag{8}$$

where A is the added-mass coefficient, k is the restoring stiffness, and F_d is the wave excitation force. Subscripts "F" and "R" represent the float and the reaction section, respectively. Note that Eq. (8) represents the steady-state response of the system induced by sinusoidal waves. The restoring stiffness k_F and k_R are equal to $\rho g S_F$ and $\rho g S_R$, where S_F and S_R are the cross-sectional area of the float and of the central column that is connected to the reaction plate. Here, the inviscid radiation added-mass and damping coefficients and the wave excitation forces used in Eq. (8) were calculated through the use of a frequency domain boundary element method (WAMIT[3]). We compared the coefficients and excitation forces from three different panel resolutions and confirmed the convergence of the WAMIT solutions.

The optimal absorbed power predicted from the RANS simulations was compared to those obtained from the theoretical solution and the potential flow solution to illustrate the difference between the solutions from each method. The results are plotted against the incident wave period in Fig. 21. For each wave period, the optimal solution obtained from the numerical simulations was determined by selecting the power absorption coefficient that provided the best power generation performance. In particular, the optimal

[3] WAMIT is a boundary element method-based code developed by WAMIT Inc. It solves the radiation and diffraction problem and is developed for modeling the linear hydrodynamic interaction between waves and various types of floating and submerged bodies.

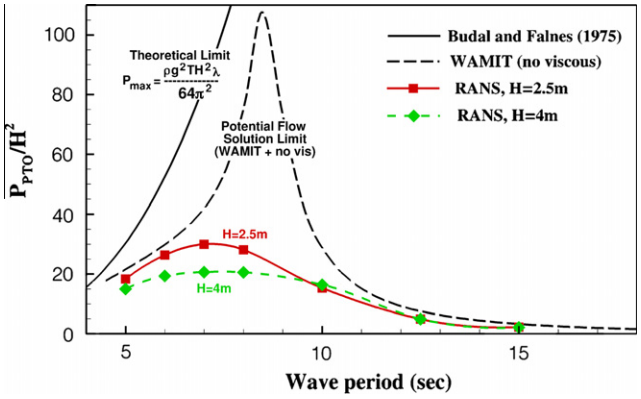

Fig. 21. Power generation of the FPA system from RANS in 2.5 m and 4 m waves (with optimal PTO absorption coefficient value).

RANS results were selected from the cases shown in Fig. 17. The results showed that, when viscosity was neglected, the two-body FPA system could have a capture width close to $\lambda/2\pi$, which was close to the analytical solution. However, in reality, the viscous drag and other nonlinear wave and floating-body interaction-induced damping forces have a significant influence on the energy capture efficiency. The difference between the power generation performance predicted by using the RANS method and the result obtained from the solution of Eq. (8) demonstrates the significance of these nonlinear damping effects.

In addition, as shown in Fig. 21, the power generation efficiency for the FPA system in 4 m waves was much lower than in 2.5 m waves. The RANS simulations revealed that the effect of the nonlinear interaction between waves and the FPA device became more significant in larger wave scenarios, where wave overtopping and the re-entering impact of out-of-water float were more significant. However, both the over topping effect and vortex shedding effect highly depend on the specification of the wave environment and the FPA design. It is not easy to quantify their effect on power output in general.

The study demonstrated that the RANS method was able to model the complex nonlinear interaction between waves and the floating body. However, RANS-based CFD simulation generally requires longer computational time. Therefore, the power performance of a WEC system is often predicted by solving the radiation and diffraction problem [25]. Viscous drag can be included in the equation of motion by adding a quadratic damping term. However, the drag coefficient value needs to be carefully selected. The selection often leads to significant uncertainty in the numerical prediction [17]. The use of RANS method here was to provide an overall understanding on the hydrodynamic and the power extraction performance of the system and to demonstrate the nonlinear effects on the performance.

6. Conclusions and future work

This paper presented a RANS study on the hydrodynamic performance of an FPA wave energy conversion system in regular waves. We also investigated the power extraction characteristics and the effect of nonlinear interaction between waves and the FPA device. A two-body FPA system was analyzed. Grid and domain size sensitivity studies were included, and a heave decay test was performed. A series of studies on the feasible value of the power absorption coefficient and the maximum power that the system can extract under various wave conditions was presented, and the results were validated with experimental data.

The results showed that the nonlinear hydrodynamic effects could have significant influence on the response of the FPA system and could reduce its power absorption efficiency. The additional nonlinear forces included the viscous drag caused by flow separation and vortex shedding, the wave overtopping force, and the impact load when the out-of-water float re-enters the water surface. These nonlinear forces no only became more significant when the wave height was larger, but could also affect the instantaneous power extraction performance in smaller wave conditions. In addition, the results revealed that the instantaneous power absorbed by the FPA system could contain high peaks and low peaks, depending on whether the FPA system was moving up or down.

The study provided insight into the complex hydrodynamic interactions of a two-body FPA system in heave and may be useful for future studies, including the investigations of optimal control and tuning of the PTO system in real seas, where the nonlinear interactions between waves and the FPA system can be more significant. Note that we did not apply any phase control strategy to the system, and the power absorption performance in the sup-resonant period region was found to decrease rapidly. The investigation of optimal control method is beyond the scope of this study but is needed in the future to improve the overall power extraction performance. Other hydrodynamic and power performance analyses are also needed, including an analysis of the effects of the mooring system and other translational/rotational motions.

Acknowledgments

We would like to acknowledge the U.S. Department of Energy's Water Power Program for supporting this work and RE Vision Consulting, LLC for collaborating on the wave tank testing.

References

[1] Thorpe TW. A brief review of wave energy. Harwell laboratory, Energy technology support unit; 1999.
[2] Cruz J. Ocean wave energy: current status and future prepectives. Springer Verlag; 2008.
[3] McCormick M. Ocean wave energy conversion. New York: Wiley-Interscience; 1981.
[4] Falcão AFO. Wave energy utilization: a review of the technologies. Renew Sustain Energy Rev 2010;14:899–918.
[5] Drew B, Plummer AR, Sahinkaya MN. A review of wave energy converter technology. Proc Institut Mech Eng A: J Power Energy 2009;223:887–902.
[6] Budal K, Falnes J. A resonant point absorber of ocean-wave power. Nature 1975;256:478–9. corrigendum 257:626.
[7] Evans DV. A theory for wave-power absorption by oscillating bodies. J Fluid Mech 1976;77:1–25.
[8] Mei CC. Power extraction from water waves. J Ship Res 1976;20:63–6.
[9] Newman JN. The interaction of stationary vessels with regular waves. In: 11th Symposium on Naval Hydrodynamics, London; 1976. p. 491–501.
[10] Budal K, Falnes J. Interacting point absorbers with controlled motion. Power from Sea Waves; 1980. p. 381–99.
[11] Falnes J. Wave-energy conversion through relative motion between two single-mode oscillating bodies. J Offshore Mech Arc Eng 1999;121:32–8.
[12] Falnes J. Ocean waves and oscillating systems. Cambridge University Press; 2002.
[13] Falnes J. A review of wave-energy extraction. Mar Struct 2007;20:185–201.
[14] Bjarte-Larsson T, Falnes J. Laboratory experiment on heaving body with hydraulic power take-off and latching control. Ocean Eng 2006;33:847–77.
[15] Korde UA. Efficient primary energy conversion in irregular waves. Ocean Eng 1999;26:625–51.
[16] Yavuz H, Stallard TJ, McCabe AP, Aggidis GA. Time series analysis-based adaptive tuning techniques for a heaving wave energy converter in irregular seas. Proc Institut Mech Eng A: J Power Energy 2007;221:77–90.
[17] Babarit A, Hals J, Muliawan MJ, Kurniawan A, Moan T, Krokstad J. Numerical benchmarking study of a selection of wave energy converters. Renew Energy 2012;41:44–63.
[18] Agamloh EB, Wallace AK, Von Jouanne A. Application of fluid-structure interaction simulation of an ocean wave energy extraction device. Renew Energy 2008;33:748–57.
[19] Bhinder MA, Mingham CG, Causon DM, Rahmati MT, Aggidis GA, Chaplin RV. A joint numerical and experimental study of a surging point absorbing wave energy converter (WRASPA). In: 28th International conference on ocean, offshore and arctic engineering, OMAE, Honolulu, HI, United States; 2009.
[20] Westphalen J, Greaves DM, Hunt-Raby A, Williams CJK, Taylor PH, Hu ZZ, et al. Numerical simulation of wave energy converters using Eulerian and

Lagrangian CFD methods. In: 20th international offshore (Ocean) and polar engineering conference, ISOPE, Beijing, China; 2010.
[21] Paixão Conde JM, Didier E. Numerical Simulation of an oscillating water column wave energy converter: comparison of two numerical codes. In: 21st International offshore (ocean) and polar engineering conference, ISOPE, Maui, Hawaii; 2011. p. 668–74.
[22] Yu Y-H, Li Y. A RANS simulation for the heave response of a two-body floating point wave absorber. In: 21st International offshore (ocean) and polar engineering conference, ISOPE, Maui, Hi, United States; 2011.
[23] Muliawan MJ, Gao Z, Moan T, Babarit A. Analysis of a two-body floating wave energy converter with particular focus on the effects of power take off and mooring systems on energy capture. In: 30th International conference on ocean, offshore and arctic engineering, OMAE, Rotterdam, The Netherlands; 2011. p. 317–28.
[24] Li Y, Yu Y-H, Epler J, Previsic M. Experimental Investigation of the power generation performance of floating-point absorber wave energy systems. In: 27th International workshop on water waves and floating bodies, Copenhagen, Denmark; 2012.
[25] Li Y, Yu YH. A synthesis of numerical methods for modeling wave energy converter-point absorbers. Renew Sustain Energy Rev 2012;16:4352–64.